

Chemical Science

Accepted Manuscript



This is an *Accepted Manuscript*, which has been through the Royal Society of Chemistry peer review process and has been accepted for publication.

Accepted Manuscripts are published online shortly after acceptance, before technical editing, formatting and proof reading. Using this free service, authors can make their results available to the community, in citable form, before we publish the edited article. We will replace this *Accepted Manuscript* with the edited and formatted *Advance Article* as soon as it is available.

You can find more information about *Accepted Manuscripts* in the [Information for Authors](#).

Please note that technical editing may introduce minor changes to the text and/or graphics, which may alter content. The journal's standard [Terms & Conditions](#) and the [Ethical guidelines](#) still apply. In no event shall the Royal Society of Chemistry be held responsible for any errors or omissions in this *Accepted Manuscript* or any consequences arising from the use of any information it contains.



www.rsc.org/chemicalscience



Journal Name

ARTICLE

Solar-Microbial Hybrid Device based on Oxygen-deficient Niobium Pentoxide Anodes for Sustainable Hydrogen Production

Mingyang Li,^a Xinjun He,^a Yinxiang Zeng,^a Meiqiong Chen,^{a,b} Ziyang Zhang,^a Hao Yang,^a Pingping Fang,^{*a} Xihong Lu,^{*a} and Yexiang Tong^{*a}

Received 00th January 20xx,
Accepted 00th January 20xx

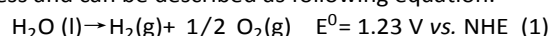
DOI: 10.1039/x0xx00000x

www.rsc.org/

Hydrogen gas is emerging as an attractive fuel with high energy density for the direction of energy resources in future. Designing integrated devices based on a photoelectrochemical (PEC) cells and a microbial fuel cell (MFC) represents a promising strategy to produce hydrogen fuel at a low price. In this work, we demonstrate a new solar-microbial (PEC-MFC) hybrid device based on the oxygen-deficient Nb₂O₅ nanoporous (Nb₂O_{5-x} NPs) anodes for sustainable hydrogen generation without external bias for the first time. Owing to the improved conductivity and porous structure, the as-prepared Nb₂O_{5-x} NPs yields a remarkable photocurrent density of 0.9 mA cm⁻² at 0.6 V (vs. SCE) in 1 M KOH aqueous solution under light irradiation, and can achieve a maximum power density of 1196 mW m⁻² when used as anode in MFC device. More importantly, a solar-microbial hybrid system by combining PEC cell with MFC is designed, in which Nb₂O_{5-x} NPs electrodes function as both anodes. The as-fabricated PEC-MFC hybrid device can simultaneously realize the electricity and hydrogen using organic matter and solar light at zero external bias. This novel design and attempt might provide a guidance for other materials to convert and store the energy.

1. Introduction

The rational utilizations of renewable and clean energy have drawn more and more attentions due to the increasing energy demands and ever-growing environmental concerns. Producing hydrogen by photoelectrochemical (PEC) water splitting over a semiconductor photoelectrode is emerging as the most promising way that can directly convert the solar energy into clean hydrogen.¹⁻³ Hydrogen from water splitting is known to be a thermodynamically uphill or endothermic process and can be described as following equation:



To drive this reaction, a minimal energy of 237.2 KJ/mol that is equal to a potential of 1.23 V vs. NHE is required.^{2,3} In this respect, it requires the conduction band (CB) and valence band (VB) edges of photoelectrode to straddle the reduction and oxidation potentials of water. Specifically, E_{CB} should be above $E_{\text{red}}(\text{H}_2/\text{H}^+)$ and E_{VB} should be below $E_{\text{ox}}(\text{OH}^-/\text{O}_2)$. Besides having suitable band edge positions, an ideal photoelectrode material for efficient solar water splitting should also possess strong light-harvesting ability, good chemical stability, fast

charge transport and low cost.⁴⁻⁶ However, most of the developed photoelectrodes cannot satisfy these requirements simultaneously. On the other hand, an external bias is always needed for practical applications to improve their charge separation and/or overcome an overpotential for the low lying CB edge, which leads to increase the cost of hydrogen production.⁷⁻¹⁰ In order to address the above-mentioned energy loss, numerous efforts have been devoted to designing nanostructured photoelectrodes and catalysts as well as optimizing the PEC configuration.¹¹⁻¹³ Nevertheless, the current efficiency of PEC water splitting is still not satisfactory for its high energy demand.^{14, 15} Alternatively, the energy required for water splitting obtained from a renewable energy source is a more cost-effective approach to generate hydrogen.

Microbial fuel cells (MFCs) are of great interest since it can directly produce electricity from organic waste and biomass in low cost. MFCs are bioelectrochemical devices that can convert chemical energy stored in organic matter into electricity by the help of microorganisms.¹⁶⁻²³ Such this feature makes them very attractive as a green energy supply to overcome the thermodynamic constraints and compensate for the energy loss of PEC water splitting. Recently, Wang *et al.* demonstrated that the hydrogen gas could be continuously produced based on solar light and biomass recycling through coupling PEC water splitting with a TiO₂ nanowire-arrayed photoanode and microbial electrohydrogenesis with *Shewanella oneidensis* MR-1 in a PEC-MFC hybrid device.¹⁶ Despite these achievements, the unsatisfactory performances of current MFCs and PEC cells are the main obstacles for their practical applications. Electrode material is the most key factor

^a KLGHEI of Environment and Energy Chemistry, MOE of the Key Laboratory of Bioinorganic and Synthetic Chemistry, School of Chemistry and Chemical Engineering, Sun Yat-Sen University, Guangzhou 510275, China. E-mail: fangpp3@mail.sysu.edu.cn (P. Fang); luxh6@mail.sysu.edu.cn (X. Lu); chedhx@mail.sysu.edu.cn (Y. Tong)

^b Dongguan Key Laboratory of Green Energy, City college of Dongguan University of Technology, Wenchang Road, Dongguan, 523419 China.

† Electronic Supplementary Information (ESI) available: Video of the generations of gas by the hybrid device under the illumination. See DOI: 10.1039/x0xx00000x

that determines the performances of both the MFCs and PEC cells.^{16-19, 24-27} Therefore, the exploration and development of advanced electrode material for improving the efficiency of PEC cells and the output power density of MFCs are highly desirable.

In this work, we demonstrate the feasibility of oxygen-deficient Nb₂O₅ nanoporous (Nb₂O_{5-x} NPs) films as high-performance anode material for both the PEC cells and MFCs. Nb₂O₅ is one of most important n-type semiconductor materials for dye-sensitized solar cells and photocatalysts in terms of its excellent photoactivity, non-toxicity and environmental friendly.²⁸⁻³³ It has similar bandgap with TiO₂ and ZnO, and favourable band-edge positions that can straddle the redox potential of water photoelectrolysis. Moreover, recent reports have shown that Nb₂O₅ possesses better biocompatibility than the TiO₂ and higher stability than ZnO (amphoteric oxide).^{34, 35} All these characteristics feature it very promising as photoanode and anode for PEC cells and MFCs, respectively. However, Nb₂O₅ suffers from poor electrical conductivity, which seriously limits its wide applications. Herein, we developed a facile approach to significantly boost the conductivity of Nb₂O₅ by creating oxygen vacancies. Nb₂O_{5-x} NPs films were readily obtained by anodic oxidation of Nb foil and hydrogenation treatment. Benefiting from the appropriate bandgap, suitable band levels, improved conductivity and well biocompatibility, the Nb₂O_{5-x} NPs exhibited superior performances in both the PEC cells and MFCs. The Nb₂O_{5-x} photoanode achieved a remarkable photocurrent density of 0.9 mA cm⁻² at 0.6 V (vs. SCE) in 1 M KOH aqueous solution, and the MFCs with Nb₂O_{5-x} NPs anodes (denoted as Nb₂O_{5-x}-MFCs) exhibited a maximum power density of 1196 mW m⁻². More interestingly, a PEC-MFC hybrid device by interfacing a Nb₂O_{5-x}-based PEC device and a Nb₂O_{5-x}-based MFC device was designed, and the continuous hydrogen gas could be produced at zero external bias by biodegradable organic matter and solar light.

2. Experimental Section

2.1 Fabrication of Nb₂O₅ and Nb₂O_{5-x} NPs

Nb₂O₅ NPs were synthesized by simple electrochemical anodization of Nb film. Before the anodization, the Nb film was washed by ultrasonication in acetone, ethanol and then deionized water successively. Nb film was anodized at an applied potential of 20 V for 30 min at room temperature, with Nb film as working electrode and a graphite rod of about 4.0 cm² as cathode in a glycerol aqueous solution (90 vol% glycerol: 10 vol% H₂O) containing 1.5% NH₄F. The as-prepared Nb₂O₅ NPs were cleaned with ethanol and DI water, and then were annealed at 450 °C for 60 min in air to enhance the mechanical stability and crystallinity. Finally, the Nb₂O_{5-x} NPs were obtained by annealing the Nb₂O₅ NPs in hydrogen atmosphere at various temperatures ranging of 450-550 °C for 60 min. Thermal treatment was performed in a home-built tube furnace filled with ultrahigh purity hydrogen gas.

2.2 Fabrication of MFC

At first, E. coli K-12 (ATCC 25922) was cultured at 37 °C fertile medium (a mixture of 10.0 peptone, 5.0 g NaCl and 3.0 g beef powder per liter) in an anaerobical test tube, which was sterilized at 121 °C in an autoclave for 20min in advance. Secondly, 10 mL E. coli K-12 culture medium was inoculated to the nitrogen saturated anolyte, after the growing for 18 h in the incubator. Cubic MFC with single chamber (4 cm × 5 cm × 5 cm) was used in this work, which consists of a polymethyl methacrylate chamber and a membrane cathode assembly on one side (4 cm × 4 cm). The sample electrodes (4 cm × 4 cm) was directly used as anode. The cathode was prepared by hot-pressing carbon paper on one side of a cation exchange membrane (CEM). The carbon paper cathode was pasted with 12.5 mg cm⁻³ commercial Pt-catalyst (40 wt% Pt/C) in a mixture of Nafion (5%). Phosphate-buffered basal medium (PBBM) with 5 mM HNQ, 10.0 g glucose and 5.0 yeast extract per liter was used as anolyte. The PBBM is constitutive of 8g NaCl, 0.2g KCl, 3.63g Na₂HPO₄·12H₂O, 0.24g KH₂PO₄ per litre. To remove the possible metal and biomass contamination, the cell was washed with 1 mol L⁻¹ HCl and 1 mol L⁻¹ NaOH and rinsed by sterile water before the inoculation.

2.3 Material Characterization

The surface structure, morphology and composition of the samples were characterized by scanning electron microscope (SEM, Quanta 400), X-ray diffraction (XRD, Bruker, D8 ADVANCE) with Cu K α radiation ($\lambda = 1.5418 \text{ \AA}$), and transmission electron microscopy (TEM, JEM2010-HR). The X-ray Photoelectron Spectroscopy (XPS, ESCALab250) with a 200W Al K α radiation was used to measure the chemical bonding state and chemical state of the samples. The C 1s peak at 284.8 eV from adventitious carbon was regarded as the energy reference. Raman spectroscopy was conducted on a Laser Micro-Raman Spectrometer (Renishaw inVia) using a visible laser ($\lambda=514.5 \text{ nm}$) with an output laser power of 50mW as the excitation wavelength at room temperature. The optical properties of the products were measured with a UV-Vis-NIR Spectrophotometer (UV, Shimadzu UV-3150). EPR spectra were studied on powdered products by a conventional Bruker spectrometer (Bruker, A300-10-12) operating at X-band frequency and magnetic field modulation of 100 kHz, with a microwave power of 2.23 mW and modulation amplitude of 8 G at 88 K. The resonance lines were simulated by the Bruker WINEPR SimFonia program.

2.4 Photoelectrochemical and Electrochemical Measurements

PEC measurements were carried out in a three-electrode cell with a flat quartz window to facilitate illumination of the photoelectrode surface. The Pt foil electrode and a saturated calomel electrode were used as counter and reference electrode, respectively. The 1.0 M NaOH aqueous solution was used as the electrolyte, and the illumination source was a 150W xenon lamp coupled with an AM 1.5G filter. Additionally 1.0 M NaOH aqueous solution with 10.0 g glucose per liter was used in the controllable experiment. Incident photon to

current conversion efficiencies (IPCE) were collected by a CHI 760D electrochemical station with a solar simulator (Newport 69920, 1000W xenon lamp), coupled with an infrared water filter (Oriol 6127) and aligned monochromator (Oriol

Cornerstone 130 1/8 m). To quantitatively reveal the interplay between the photoactivity and light absorption, incident photon to current

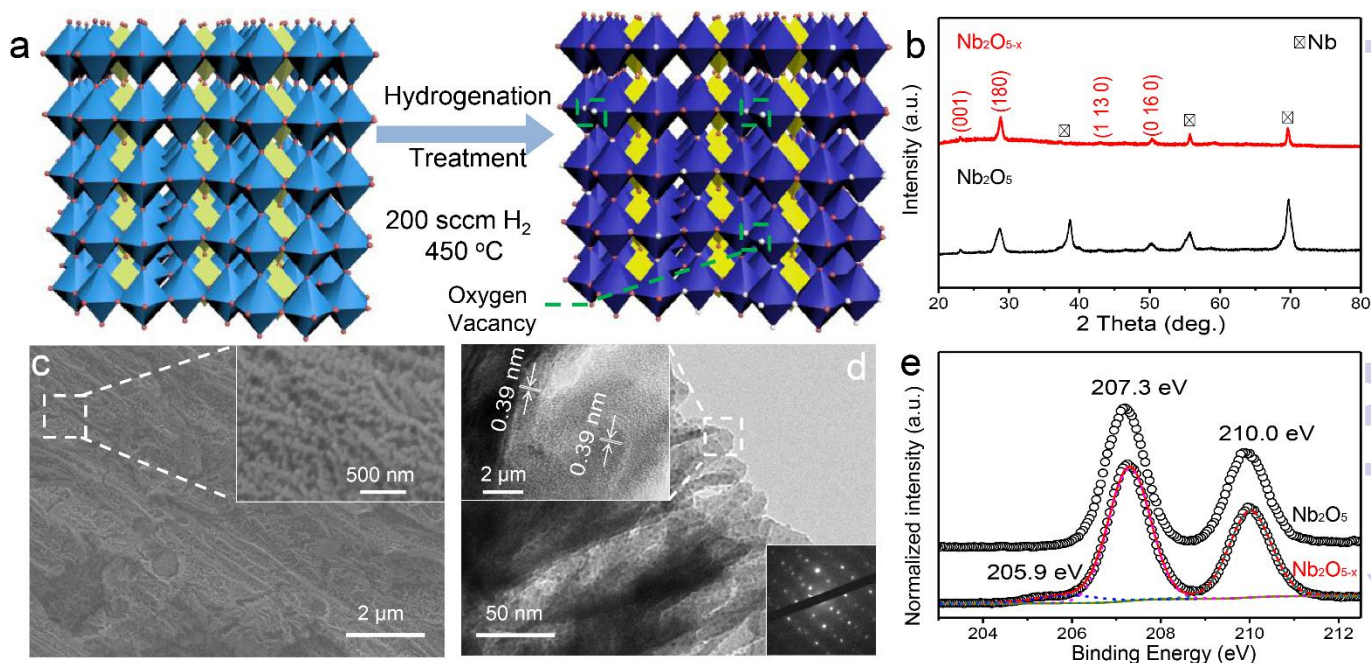


Figure 1. (a) Crystal structure of Nb₂O₅ and showing the formation of oxygen vacancies; (b) XRD spectra of Nb₂O_{5-x} NPs; (c) SEM images of Nb₂O_{5-x} NPs; inset: magnified SEM image of Nb₂O_{5-x} NPs; (d) TEM images of Nb₂O_{5-x} NPs; the upper left inset: lattice-resolved TEM image collected at the edge of the NP; the bottom right inset: the diffraction pattern; (e) Normalized Nb 3d core-level XPS spectra collected for Nb₂O₅ and Nb₂O_{5-x} NPs.

conversion efficiency (IPCE) were measured on Nb₂O₅ and Nb₂O_{5-x} NPs photoanodes at 0.2 V vs. SCE. IPCE can be expressed by the equation:

$$\text{IPCE} = (1240I) / (\lambda J_{\text{light}}) \quad (2)$$

Where I is the measured photocurrent density at a specific wavelength, λ is the wavelength of incident light, and J_{light} is the measured irradiance at a specific wavelength. The conductivity of the as-prepared films is measured by two-point current-potential (I - V) curves (LSV) by a typical two electrode system. One of the electrodes is fixed on the substrate and the other fixed on the surface of the film. All the process is completed with the silver paste and under the same condition.

3. Results and Discussion

3.1 Synthesis and Characterization of Nb₂O_{5-x} NPs

Nb₂O_{5-x} NPs were obtained through a two-step procedure, which involves anodic oxidation of Nb foil and heat treatment in hydrogen atmosphere. Firstly, Nb₂O₅ NPs films were synthesized on a niobium film substrate by a simply anodic oxidation method and annealed in air at 450 °C (Experimental Section). SEM images show that the white homogeneous film obtained on the metal substrate is composed of dense nanoporous arrays with ~50 nm diameter (Figure S1, Supporting Information). Then, to introduce oxygen vacancies into Nb₂O₅ NPs, the as-prepared Nb₂O₅ NPs were then annealed in hydrogen atmosphere for an additional 60 min at

500 °C. The synthetic process of hydrogen treatment is illustrated as Figure 1a. After the treatment, the film colour changed from white to blue (Figure S2, Supporting Information), suggesting the possible modification in the crystal structure. To identify the possible phase transformation, XRD patterns of the Nb₂O₅ and Nb₂O_{5-x} NPs are collected in Figure 1b. The sharp diffraction peaks centered at 2 θ angles of 22.6°, 28.4° and 50.8°, corresponding to the (001), (180) and (016 0) planes of Nb₂O₅ (JCPDS #30-0873), are observed for both the samples, indicating that the NPs are well crystalline with similar phase. SEM studies also reveal there are no obvious morphological changes for Nb₂O_{5-x} NPs after the hydrogenation (Figure 1c). Figure 1d displays the TEM analysis and selected-area electron diffraction (SAED) of Nb₂O_{5-x} NPs. TEM analysis obviously shows the porous Nb₂O_{5-x} sample consists of the nanoporous arrays. The clear lattice fringes with spacing of 0.39 nm is indexed to the (001) plane of orthorhombic Nb₂O₅ samples. Meanwhile, the bright and well-arranged diffraction spots further confirm the high crystalline nature of the Nb₂O_{5-x} NPs.

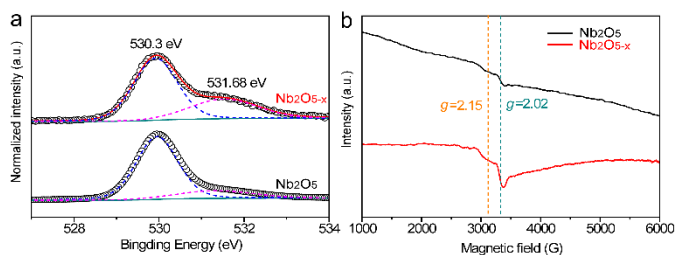


Figure 2. (a) Normalized O 1s core-level XPS and (b) EPR spectra collected for Nb₂O₅ and Nb₂O_{5-x} NPs.

UV-visible absorption spectra of Nb₂O₅ and Nb₂O_{5-x} NPs were collected to investigate the influence of hydrogenation on the optical absorption (Figure S2, Supporting Information). Both the samples exhibit similar light absorption in the UV region and the Nb₂O_{5-x} NPs show substantially higher absorption compared to pristine Nb₂O₅ in the region of 400–800 nm, which suggests the Nb₂O_{5-x} may absorb more visible light. The band gap of the Nb₂O_{5-x} NPs is calculated to be 3.26 eV, while 3.35 eV for the pristine Nb₂O₅ NPs, indicating the hydrogenation has negligible effects on its band gap. To further investigate the effect of hydrogen treatment on the chemical state of Nb₂O₅, XPS analysis was performed. The XPS survey of Nb₂O_{5-x} NPs was collected to prove no other impurities were introduced after the hydrogen treatment (Figure S3, Supporting Information). Figure 1e displays the normalized high resolution Nb 3d core level XPS spectra. Both the samples have two peaks located at 207.3 and 210 eV, which are ascribed to the regular Nb 3d signals for Nb⁵⁺.^{36, 37} Remarkably, the Nb₂O_{5-x} NPs displays an additional peak emerged at the lower binding energy of 205.9 eV, which is the typical peak position for the low charge Nb⁴⁺.³⁸⁻⁴⁰ The presence of Nb⁴⁺ in Nb₂O_{5-x} NPs also had been regarded as the reason why the film colour changed from white to blue after the hydrogenation (Figure S2, Supporting Information).⁴¹⁻⁴³ Figure 2a compares the normalized O 1s core level XPS spectra of Nb₂O₅ and Nb₂O_{5-x} NPs. Significantly, the Nb₂O_{5-x} NPs shows a broader peak at around 531.68 eV than that of Nb₂O₅ NPs, indicating it has more oxygen vacancies than Nb₂O₅ NPs.^{40, 44-48} This is also confirmed by electron paramagnetic resonance (EPR) analysis. The broader peaks at $g=2.15$ and 2.02 in Figure 2b clearly reveals the density of oxygen vacancy in Nb₂O_{5-x} NPs is much higher than that in the Nb₂O₅ NPs.^{49, 50}

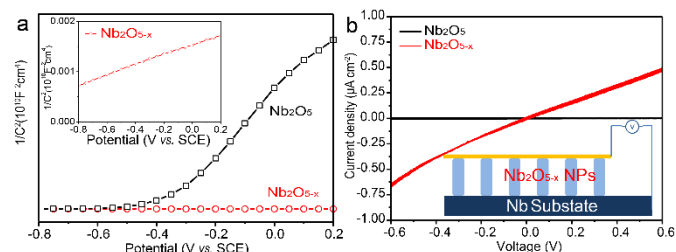


Figure 3. (a) Mott-Schottky plots of Nb₂O₅ and Nb₂O_{5-x} NPs at a frequency of 1 kHz in the dark; (b) Comparison of I - V curves of the samples; the inset is the schematic of the measurement.

Electrochemical impedance measurements were carried out to verify our hypothesis that the induced oxygen vacancy can serve as shallow donor to increase carrier density of Nb₂O₅. Figure 3a displays the Mott-Schottky plots of the electrodes at a frequency of 1 kHz in the dark, which are generated based on capacitances that derived from the electrochemical impedance. Both the Nb₂O₅ and Nb₂O_{5-x} NPs show positive slopes, in line with the characteristic of n -type semiconductor. Notably, Nb₂O_{5-x} NPs shows substantially smaller slope of Mott-Schottky plot than Nb₂O₅ NPs, suggesting significantly increased donor densities based on the following equation:

$$N_d = (2/e_0\epsilon\epsilon_0) [d(1/C^2)/dV]^{-1} \quad (3)$$

where N_d is the donor density, e_0 the electron charge, ϵ the dielectric constant of Nb₂O₅ ($\epsilon=41$), ϵ_0 the permittivity of vacuum, and V the applied bias at the electrode.⁴¹ The carrier densities of the Nb₂O₅ and Nb₂O_{5-x} samples are calculated to be 1.45×10^{18} and 3.68×10^{23} cm⁻³, respectively. It should be pointed that we here used the electrode area instead of the surface area of the nanoporous film for the calculation, which may cause errors in determining the carrier densities. However, a qualitative comparison of carrier densities between the Nb₂O₅ and Nb₂O_{5-x} NP samples is reliable, since they have similar morphology and surface area. Obviously, the Nb₂O_{5-x} NPs possess 5 order of magnitude improvement on donor density compared to the Nb₂O₅ NPs, resulting in significantly facilitating charge separation in the Nb₂O_{5-x} NPs. Meanwhile, the I - V curves of Nb₂O₅ and Nb₂O_{5-x} NPs at room temperature were also collected in Figure 3b. As expected, the electrical conductivity of the Nb₂O₅ sample is substantially improved after hydrogenation. All these results validly confirm that the introduced oxygen vacancies can remarkably enhance the donor density as well as the conductivity of the Nb₂O₅ NPs.

3.2 Performances of PEC devices based on Nb₂O_{5-x} Photoanodes

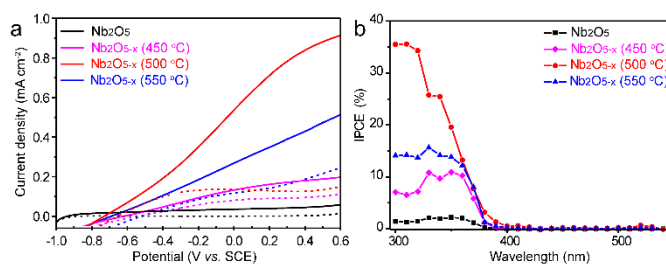


Figure 4. (a) I - V curves measured under 100 mW cm^{-2} simulated solar light generated by a 100 W xenon lamp coupled with an AM 1.5G filter in 1 M NaOH electrolyte; (b) IPCE spectra measured at 0.2 V vs. SCE in 1 M NaOH electrolyte.

The PEC performances of the Nb₂O₅ samples were measured in a three electrode electrochemical cell with 1.0 M NaOH solution as electrolyte. For optimizing the PEC performance of Nb₂O_{5-x} NPs, the effect of the hydrogenation temperature was studied. Figure 4a shows the linear sweep curves (LSV) of the pristine Nb₂O₅ and Nb₂O_{5-x} NPs obtained at different hydrogenation temperatures. The photocurrent density of Nb₂O₅ NPs is 0.05 mA cm^{-2} at 0.6 V vs. SCE, which is closed to the value reported previously.³⁶ The photocurrent densities of Nb₂O_{5-x} NPs increase gradually with the increasing of hydrogen

treatment temperature from 450 to 500 °C. The Nb₂O_{5-x} (500 °C) NPs achieves a maximum value of 0.9 mA cm⁻² at 0.6 V vs. SCE, which is about 20-fold enhancement compared to Nb₂O₅ NPs at the same potential. This photocurrent density is also dramatically higher than the values recently reported for the reported values of Nb₂O₅ photoanodes, such as N-doped Nb₂O₅ nanostructures (Table S1).^{36, 51-53} Photocurrent densities decrease gradually with the rising temperature when the annealing temperature is above 500 °C. According to the increasing donor density and conductivity of the Nb₂O_{5-x} with the rising hydrogenation temperature (Figure S4, Supporting Information), it can be concluded that the excessive oxygen vacancies will serve as the recombination centre for electron and hole, resulting in a poor PEC performance, which also agrees with other works.⁵⁴ To quantitate the interplay between the photoactivity and light absorption, incident photon to current conversion efficiency (IPCE) were measured on Nb₂O₅ and Nb₂O_{5-x} NPs photoanodes at 0.2 V vs. SCE (Figure 4b). All the Nb₂O_{5-x} NPs shows significantly enhanced photoactivity over the entire UV region, and the Nb₂O_{5-x} NPs hydrogenated at 500 °C exhibits the best IPCE efficiency in the wavelength range from 300 to 380 nm. Additionally, the IPCE values decrease from 35 % at 300 nm to 1 % at 400 nm, and we did not observe any photoactivity in the visible light region beyond 400 nm, indicating that the observed colour change is not because of the band gap modification of Nb₂O₅ or the transition between the impurity states and conduction/valence band edges.⁴⁷ Thus, we believe that the photoactivity enhancement of the Nb₂O_{5-x} NPs is because of the increased donor density and conductivity originating from the induced oxygen vacancies generated during the hydrogenation.

3.3 Performances of the MFC devices based on the Nb₂O_{5-x} Anodes

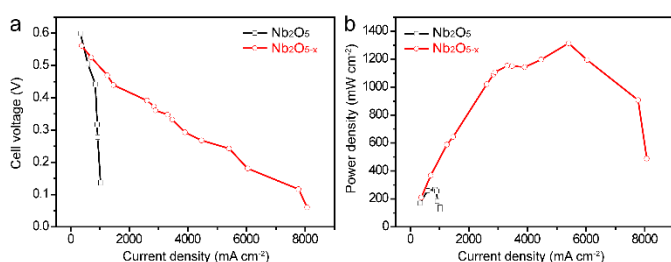


Figure 5. Comparisons of (a) polarization curves and (b) power outputs for Nb₂O₅ and Nb₂O_{5-x} anodes.

To demonstrate that the as-prepared Nb₂O_{5-x} NPs film is also a promising candidate as high-performance anode material for MFC device, a simple MFC device was assembled using the Nb₂O_{5-x} NPs hydrogenated at 500 °C as anode and a 40 wt% Pt/C loaded carbon paper as air cathode in the *E. coli* MFCs (denoted as Nb₂O_{5-x}-MFC, Experimental Section). For better comparison, the performance of the pristine Nb₂O₅ NPs film in MFC device was also measured (denoted as Nb₂O₅-MFC). Figure 5a and 5b depict the comparison of polarization curves and power outputs tested by loading various external resistances. In comparison to Nb₂O₅-MFC, the cell voltage of

Nb₂O_{5-x}-MFC decreased more slowly with the decreased loaded resistance and gently, indicating the superior performance of the Nb₂O_{5-x} NPs anode. Furthermore, the Nb₂O_{5-x}-MFC achieved a remarkable maximum power density of 1196 mW m⁻² at a current density of 4465 mA m⁻², which is substantially higher than that of Nb₂O₅-MFC (140 mW m⁻²). The distinct enhancement between the Nb₂O₅ and Nb₂O_{5-x} MFC devices can be ascribed to the superior conductivity of Nb₂O_{5-x} NPs anode. Additionally, Without *E. coli*, the Nb₂O_{5-x}-MFC device show negligible cell voltage and output power density when loading the external resistances (Figure S5), indicating *E. coli* is very important for power production.

3.4 Performances of PEC-MFC hybrid devices based on Nb₂O_{5-x} Anodes

For taking a full advantage of the oxygen-deficient electrodes, we assembled a PEC-MFC hybrid device to convert and store the energy using both Nb₂O_{5-x} NPs. (Experimental Section) The PEC properties of Nb₂O_{5-x} NPs were measured in a two-electrode electrochemical cell with/without MFC devices in the dark and under 1 sun illumination. Figure 6a shows the schematic configuration of the integrated PEC-MFC hybrid device. By coupling the PEC and MFC devices in series, the Nb₂O_{5-x} anode in MFC provides a biovoltage that shifted the potential of the illuminated Nb₂O_{5-x} photoanode near -0.6 V, thus, enabling the water splitting to occur at zero external bias (Figure 6b). The PEC-MFC device displays a novel photocurrent density of 0.18 mA cm⁻² at zero bias (0 V vs. Pt), which is substantially larger than the one obtained from the PEC alone at the same potential (Figure 6b). More importantly, gas bubbles were clearly observed to be continuously evolving on the Pt electrode under the light illumination (Figure S6 and Video S1, Supporting Information), indicating the generations of hydrogen. Meanwhile, the PEC device in the presence of

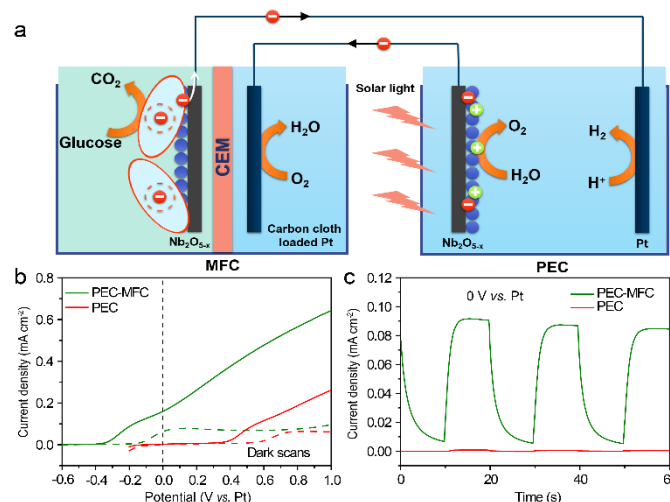


Figure 6. (a) Schematic configuration of a PEC-MFC device; (b) *I-V* curves collected from a PEC device (red line) and a PEC-MFC device (olive line) with the Nb₂O_{5-x} NPs electrodes at a scan rate of 10 mV/s with/without the white light illumination; (c) *I-T* curves recorded for the PEC device (red line) and the PEC-MFC device (olive line) at 0 V vs. Pt, with light on/off cycles.

glucose, possessing a lower performance than the hybrid device, was also conducted to emphasize the excellent energy efficiency via this PEC-MFC hybrid device. (Figure S7) There is no doubt that the Nb₂O_{5-x} NPs is an outstanding materials to integrate the merits in both the PEC and MFC and the hybrid device is an efficient strategy to convert and store the energy. The PEC-MFC device also exhibits reproducible photocurrent generation in response to light illumination (Figure 6c), implying the hybrid device is feasible to produce the hydrogen. To the best of our knowledge, this is the first demonstration of using PEC-MFC hybrid devices based on the same anode material to generate hydrogen at zero external bias.

4. Conclusions

In summary, we developed a facile and effective method to significantly improve the conductivity and performances of the Nb₂O_{5-x} NPs in PEC cells and MFCs through the introduction of oxygen vacancies. The Nb₂O_{5-x} NPs photoanode achieved a remarkable photocurrent density of 0.9 mA cm⁻² at 0.6 V (vs. SCE) in 1 M KOH aqueous solution. Meanwhile, the Nb₂O_{5-x}-MFC exhibited a superior power density of 1196 mW m⁻² when the Nb₂O_{5-x} NPs was used as an anode in the MFC cell. The oxygen vacancy plays a critical role in enhancing the effective charge transport of electrodes, as well as increasing the conductivity. Moreover, we also demonstrated that the PEC-MFC hybrid device with the Nb₂O_{5-x} NPs anodes in the both devices are feasible and could produce hydrogen even at zero external bias (0 V vs. Pt) under the illumination. To our best knowledge, it is the first report about the applications of Nb₂O₅ materials in the integrated PEC-MFC device to produce the hydrogen without an external bias, just using organic matter and solar light. This environmental and novel design provides a promising research direction for the future development of energy conversion and storage.

Acknowledgements

This work was supported by the Natural Science Foundations of China (21476271, 2141101037, 21403306, and J1103305), Guangdong Natural Science Foundation for Distinguished Young Scholar (2014A030306048), the Research Fund for the Doctoral Program of Higher Education of China (20120171110043), and the Fundamental Research Foundations for the Central Universities (15lgpy24).

Notes and references

1. A. Fujishima and K. Honda, *Nature*, 1972, **238**, 37-38.
2. X. Wang, K. Q. Peng, Y. Hu, F. Q. Zhang, B. Hu, L. Li, M. Wang, X. M. Meng and S. T. Lee, *Nano Lett.*, 2014, **14**, 18-23.
3. S. C. Riha, B. M. Klahr, E. C. Tyo, S. Seifert, S. Vajda, M. J. Pellin, T. W. Hamann and A. B. Martinson, *ACS Nano*, 2013, **7**, 2396-2405.
4. Y. Ling, G. Wang, J. Reddy, C. Wang, J. Z. Zhang and Y. Li, *Angew. Chem. Int. Edit.*, 2012, **124**, 4150-4155.
5. Y. Hou, F. Zuo, A. Dagg and P. Feng, *Angew. Chem. Int. Edit.*, 2013, **52**, 1248-1252.
6. Y. Qiu, S. F. Leung, Q. Zhang, B. Hua, Q. Lin, Z. Wei, K. H. Tsui, Y. Zhang, S. Yang and Z. Fan, *Nano Lett.*, 2014, **14**, 2123-2129.
7. S. J. A. Moniz, S. A. Shevlin, D. J. Martin, Z.-X. Guo and J. Tang, *Energ. Environ. Sci.*, 2015, **8**, 731-759.
8. D. K. Bora, A. Braun, R. Erni, U. Müller, M. Döbeli and E. C. Constable, *Phys. Chem. Chem. Phys.*, 2013, **15**, 12648-12659.
9. K. Li, R. Chen, S.-L. Li, M. Han, S.-L. Xie, J.-C. Bao, Z.-H. Dai and Y.-Q. Lan, *Chem. Sci.*, 2015, **6**, 5263-5268.
10. J. Willkomm, N. M. Muresan and E. Reisner, *Chem. Sci.*, 2015, **6**, 2727-2736.
11. Z. Li, W. Luo, M. Zhang, J. Feng and Z. Zou, *Energ. Environ. Sci.*, 2013, **6**, 347-370.
12. X. Lang, X. Chen and J. Zhao, *Chem. Soc. Rev.*, 2014, **43**, 473-486.
13. X. Lu, S. Xie, H. Yang, Y. Tong and H. Ji, *Chem. Soc. Rev.*, 2014, **43**, 7581-7593.
14. J. Liu, Y. Liu, N. Liu, Y. Han, X. Zhang, H. Huang, Y. Lifshitz, S. T. Lee, J. Zhong and Z. Kang, *Science*, 2015, **347**, 970-974.
15. C. Mao, F. Zuo, Y. Hou, X. Bu and P. Feng, *Angew. Chem. Int. Edit.*, 2014, **53**, 10485-10489.
16. H. Wang, F. Qian, G. Wang, Y. Jiao, Z. He and Y. Li, *ACS Nano*, 2013, **7**, 8728-8735.
17. F. Qian, H. Wang, Y. Ling, G. Wang, M. P. Thelen and Y. Li, *Nano Lett.*, 2014, **14**, 3688-3693.
18. F. Qian, G. Wang and Y. Li, *Nano Lett.*, 2010, **10**, 4686-4691.
19. Y. Qiao, S. J. Bao, C. M. Li, X. Q. Cui, Z. S. Lu and J. Guo, *ACS Nano*, 2008, **2**, 113-119.
20. B. E. Logan, B. Hamelers, R. Rozendal, U. Schroder, J. Keller, S. Freguia, P. Aelterman, W. Verstraete and K. Rabaey, *Environ. Sci. Technol.*, 2006, **40**, 5181-5192.
21. R. S. Berk and J. H. Canfield, *Appl. Microbiol.*, 1964, **12**, 10-12.
22. J. B. Davis and H. F. Yarbrough, *Science*, 1962, **137**, 615-616.
23. S. J. Yuan, G. P. Sheng, W. W. Li, Z. Q. Lin, R. J. Zeng, Z. H. Tong and H. Q. Yu, *Environ. Sci. Technol.*, 2010, **44**, 5575-5580.
24. T. W. Kim and K. S. Choi, *Science*, 2014, **343**, 990-994.
25. Y. M. Ma, S. R. Pendlebury, A. Reynal, F. Le Formal and J. R. Durrant, *Chem. Sci.*, 2014, **5**, 2964-2973.
26. J. A. Turner, *Science*, 2013, **342**, 811-812.
27. H. Li, Y. Zhou, W. Tu, J. Ye and Z. Zou, *Adv. Funct. Mater.*, 2015, **25**, 998-1013.
28. S.-q. Guo, X. Zhang, Z. Zhou, G.-d. Gao and L. Liu, *J. Mater. Chem. A*, 2014, **2**, 9236-9243.
29. M. Catti and M. R. Ghaani, *Phys. Chem. Chem. Phys.*, 2014, **16**, 1385-1392.
30. Z. Wang, J. Hou, C. Yang, S. Jiao, K. Huang and H. Zhu, *Phys. Chem. Chem. Phys.*, 2013, **15**, 3249-3255.
31. G. Li, X. Wang and X. Ma, *J. Mater. Chem. A*, 2013, **1**, 12409-12412.
32. H. Luo, W. Song, P. G. Hoertz, K. Hanson, R. Ghosh, S. Rangan, M. K. Brennaman, J. J. Concepcion, R. A. Binstead, R. A. Bartynski, R. Lopez and T. J. Meyer, *Chem. Mater.*, 2013, **25**, 122-131.
33. C. N. Carvalho, J. R. Martinelli, J. Bauer, M. Haapasalo, Y. Shen, V. Bradaschia-Correa, A. P. Manso and G. Gavini, *Int. Endod. J.*, 2015, **48**, 451-459.
34. D. Velten, E. Eisenbarth, N. Schanne and J. Breme, *J. Mater. Sci. Mater. M.*, 2004, **15**, 457-461.
35. E. Eisenbarth, D. Velten, M. Muller, R. Thull and J. Breme, *J. Biomed. Mater. Res. A*, 2006, **79**, 166-175.

36. T. Ruff, R. Hahn, M. S. Killian, H. Asoh, S. Ono and P. Schmuki, *Electrochim. Acta*, 2012, **62**, 402-407.
37. X. Wang, G. Chen, C. Zhou, Y. Yu and G. Wang, *Eur. J. Inorg. Chem.*, 2012, **2012**, 1742-1749.
38. B. Gao, J. Fu, K. Huo, W. Zhang, Y. Xie and P. K. Chu, *J. Am. Ceram. Soc.*, 2011, **94**, 2330-2338.
39. J. F. Moulder, W. F. Stickle, P. E. Sobol and K. D. Bomben, *Handbook of X-ray photoelectron spectroscopy*, Perkin Elmer Eden Prairie, MN, 1992.
40. W. P. Chen, K. F. He, Y. Wang, Y. M. Hu, J. L. Cao and H. L. W. Chan, *Jpn. J. Appl. Phys.*, 2010, **49**, 051103.
41. M. R. N. Soares, S. Leite, C. Nico, M. Peres, A. J. S. Fernandes, M. P. F. Graça, M. Matos, R. Monteiro, T. Monteiro and F. M. Costa, *J. Eur. Ceram. Soc.*, 2011, **31**, 501-506.
42. F. Vratny and F. Micale, *Transactions of the Faraday Society*, 1963, **59**, 2739-2749.
43. M. Wertheimer and J. Bailon, *J. Vac. Sci. Technol.*, 1977, **14**, 699-704.
44. N. Özer, T. Barreto, T. Büyüklımanlı and C. M. Lampert, *Sol. Energ. Mat. Sol. C.*, 1995, **36**, 433-443.
45. A. L. Viet, M. V. Reddy, R. Jose, B. V. R. Chowdari and S. Ramakrishna, *J. Phys. Chem. C*, 2010, **114**, 664-671.
46. M. Li, Y. Hu, S. Xie, Y. Huang, Y. Tong and X. Lu, *Chem. Commun.*, 2014, **50**, 4341-4343.
47. G. Wang, H. Wang, Y. Ling, Y. Tang, X. Yang, R. C. Fitzmorris, C. Wang, J. Z. Zhang and Y. Li, *Nano Lett.*, 2011, **11**, 3026-3033.
48. X. Lu, G. Wang, T. Zhai, M. Yu, J. Gan, Y. Tong and Y. Li, *Nano Lett.*, 2012, **12**, 1690-1696.
49. R. Brayner and F. Bozon-Verduraz, *Phys. Chem. Chem. Phys.*, 2003, **5**, 1457-1466.
50. F. Dolci, M. D. Chio, M. Baricco and E. Giamello, *J. Mater. Sci.*, 2007, **42**, 7180-7185.
51. H. Dong, G. Chen, J. Sun, Y. Feng, C. Li and C. Lv, *Chem. Commun.*, 2014, **50**, 6596-6599.
52. J. Jiang, M. Wang, Q. Chen, S. Shen, M. Li and L. Guo, *RSC Adv.*, 2014, **4**, 10542-10548.
53. H. Miyake and H. Kozuka, *J. Phys. Chem. B*, 2005, **109**, 17951-17956.
54. Y. Yang, Y. Ling, G. Wang and Y. Li, *Eur. J. Inorg. Chem.*, 2014, **2014**, 760-766.